THE USE OF $(Mg_{0.9}Zn_{0.1})TiO_3$+2wt.% Bi_2O_3 CERAMICS AS A DIELECTRIC RESONATOR OSCILLATOR MATERIAL AND CHARACTERISATION OF STRUCTURE, MICROSTRUCTURE, AND DENSITY

Afandy Kadarosman, Frida U. Ermawati*

Department of Physics, Universitas Negeri Surabaya
Jl. Ketintang Campus, Surabaya 60231 Indonesia

Received: 23rd February 2021; Revised: 6th April 2021; Accepted: 28th April 2021

ABSTRACT

Magnesium titanate ($MgTiO_3$)-based ceramics have the potential for use in the telecommunications industry at microwave frequencies, including as a resonator in dielectric resonator oscillator (DRO) circuit. This research is intended to study the application of $(Mg_{0.9}Z_{0.1})TiO_3$+2wt.% Bi_2O_3 (abbreviated MZT01-2) ceramics as DRO material and characterize the structure, microstructure, and bulk density. Fabrication was carried out by ball milling between $(Mg_{0.9}Z_{0.1})TiO_3$ crystalline powder and 2wt.% Bi_2O_3 powder. The milled powder was compacted at certain pressure using a die press to become pellets. All pellets were sintered at 1000, 1100, 1200°C for 4 h to obtain ceramics. The structural characterization using XRD showed that the three ceramics contained the main $MgTiO_3$ phase, each 93.63, 93.83, and 90.78% molar, the rest was the $MgTi_2O_5$ phase. The increase in sinter temperature causes the lattice parameter and the unit cell volume to decrease. The Archimedes bulk density was 2.928; 2.832 and 2.736 g/cm^3. The microstructure is solid surfaces with a grain diameter of 1.9-2.3 μm accompanied by pores. As DRO materials, the three ceramics exhibited a resonant frequency at 5.11, 5.08, and 5.12 GHz which shows that the ceramics can be applied as DRO materials at microwave frequencies. The sinter temperature variation tends not to affect the resonant frequency position.

Keywords: DRO materials; Resonance frequencies; MZT01-2 ceramics; Structure; Microstructure

Introduction

The microwave frequency telecommunication industry in mobile telecommunication systems, satellite transmitters, radar detectors, global positioning systems (GPS), and dielectric oscillator resonators (DRO) has grown rapidly.[1] To support the progress of the telecommunication industry, a ceramic dielectric material is needed to be used as an electronic component material. Therefore, the fabrication of dielectric ceramic material is growing rapidly, including fabrication of magnesium titanate ($MgTiO_3$)-based dielectric ceramics.

$MgTiO_3$-based dielectric ceramics have superior dielectric properties, as reported by Wu et al[2] i.e. relative permittivity value (ε_r) ~17.8, quality factor ($Q\times f$) ~156.300 GHz and temperature coefficient at the resonance frequency (τ_f) is near to zero ~ -44.2 ppm/°C. Further reported by Wang et al[3] that $MgTiO_3$ ceramics have ε_r ~17.6, $Q\times f$ ~33.768 GHz, and τ_f near to zero. It was later reported by Zhang et al[4] that $MgTiO_3$ ceramics have ε_r ~18,38. With these properties, $MgTiO_3$ dielectric ceramics have the potential to be used as electronic component materials for the microwave telecommunication industry, one of them is as dielectric resonator oscillator (DRO) elements/materials.

DRO element is a dielectric ceramic material designed as a resonator operating in the microwaves region.[5] The principle and function of a dielectric ceramic material as the resonator is similar to the resonator cavity.[6]

*Corresponding Author.
E-Mail: frida.ermawati@unesa.ac.id

Microwaves are maintained inside the resonator material by supplying irregular permittivity value changes on the resonator surface and microwaves will bounce back and forth between the sides on the walls of the resonator.[7] At a certain frequency, namely the resonance frequency, the microwave will form a standing wave in the resonator. These standing waves will oscillate with a large amplitude.[8] The main use of dielectric resonators on DRO circuits serves to control the generated radio waves.[9]

There are two types of DRO for microwave applications, namely magnetic transverse (TM) mode and electric transverse (TE) mode.[10] In this case, only TE mode is discussed. A TE mode is a waveguide mode that depends on a transverse electric wave, usually called an H (magnetic) wave because there is only a magnetic field along its propagation direction, considering that the direction of the electric field (E) is always perpendicular to the direction of propagation. TE_{01} is selected in DRO element design because TE_{01} mode is most commonly used in rectangular waveguides and has a low resonance mode.[11,12]

The resonance frequency (f_o) in the TE_{01} mode can be calculated by Equation (1).[13]

$$f_o(\text{GHz}) = \frac{8.553}{\sqrt{\varepsilon_r}\left(\frac{\pi}{4}d^2h\right)^{1/3}} \quad (1)$$

where d is resonator diameter, and h is resonator thickness, ε_r is resonator dielectric constant. According to Ermawati et al,[14] the dimension scheme of a DRO material used in Equations (1), as well as the equivalence circuit is shown in Fig. 1.

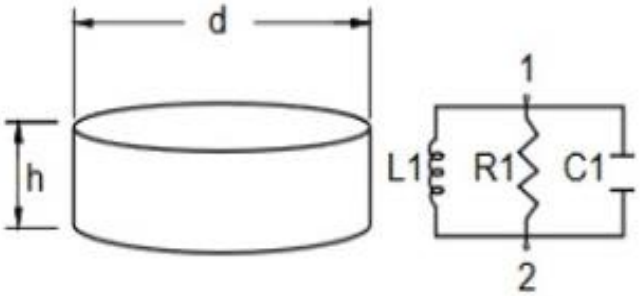

Figure 1. Dimension of a DRO material and its equivalence circuit. The diameter (d) and thickness (h) are in mm order, i.e. d = 5 mm, h = ~1-1.5 mm.[14]

A block diagram of DRO circuit consists of four parts, namely: 1) *a dielectric material*, in this case, a dielectric ceramic that acts as a resonator, 2) *a stripline* is a metal waveguide made of copper as a transmission line of electromagnet wave to produce a resonance frequency in the tested ceramic according to Equation (1), 3) *a matching network* is a matching impedance circuit to ensure matching between the transmission line input impedance and the output impedance (Z_{in}=Z_{out}) so that the power transfer occurs maximum and 4) *a feedback element* which is a feedback circuit to ensure that the stability factor of the active device is less than one for the system to work steadily.[14,15]

Meanwhile, a block diagram of DRO resonance frequency measurement of a dielectric ceramic consists of three parts i.e.[14,15] 1) *a DRO circuit* as mentioned previously, 2) *a power supply* serves to provide voltage to the DRO, typically 12 Volts and 3) *a spectrum analyzer* serves to read the output signal from the DRO, i.e. the resonance frequency signal at a certain output power.

Fabrication of $MgTiO_3$-based ceramics has been reported by several authors, one of them is by Rostianbudi and Ermawati[16] who fabricated $(Mg_{0.5}Zn_{0.5})TiO_3$ ceramics by adding the various composition of 1, 3, 5, and 7 wt.% Bi_2O_3 and sintered the ceramics at 1000°C for 2 h. It was reported that $MgTiO_3$ was detected as the main phase in the ceramics but still found secondary phase of Mg_2TiO_4 and TiO_2 rutile as impurity phase. The increase of wt.% Bi_2O_3 addition causes an increase in the bulk density of the ceramics.

Further was by Rettiningtyas and Ermawati[17] $(Mg_{0.8}Zn_{0.2})TiO_3$+2wt.% Bi_2O_3 ceramics were fabricated by varying sintering holding times for 4, 6, and 8 h at 1100°C. The main phase of $MgTiO_3$ was also identified accompanied by a minor $MgTi_2O_5$ phase. The bulk density of the ceramics relatively increased along with the sintering holding time.

The next was reported by Zendya and Ermawati[18] fabrication of $(Mg_{0.9}Zn_{0.1})TiO_3$+2wt.% Bi_2O_3 ceramics were carried out by varying compaction pressure at 10, 15, and 20 MPa and sintered the ceramics at 1100°C for 4 h. $MgTiO_3$ phase was detected almost as a single-phase and leaving a small fraction of TiO_2 rutile. Finally, Nisa and Ermawati[19] reported the fabrication of $(Mg_{0.6}Zn_{0.4})TiO_3$ ceramics by adding 1 and 5 wt.% Bi_2O_3 and sintered the ceramics at 1000°C for 4 h. The $mgTiO_3$ phase was identified as the main phase accompanied by the MgO phase as an impurity. The ceramic bulk density was in line with the increase of Bi_2O_3 content. For all of the above publications, the characterization of $(Mg_{1-x}Zn_x)TiO_3$ ceramics was limited to structure, microstructure, and density. Attempts to examine the use of ceramics as a DRO resonator material have not been reported.

Based on that, this paper is intended to report the fabrication of $(Mg_{0.9}Zn_{0.1})TiO_3$+2wt.% Bi_2O_3 (abbreviated MZT01-2) ceramics and examine the potential use of the ceramics as a resonator material in a DRO circuit operating in microwaves region, as well as to characterize the structure, microstructures, and bulk density. The ceramics were sintered at three different temperatures, i.e. 1000, 1100, and 1200°C each for 4 h.

Methods

1. Ceramic Fabrication

The starting materials used in this study are ready-to-use $(Mg_{0.9}Zn_{0.1})TiO_3$ crystalline powder (abbreviated MZT01) and 2wt.% Bi_2O_3 powder (Merck). Fabrication of MZT01+2 wt.% Bi_2O_3 ceramics (abbreviated MZT01-2) was carried out by mixing the MZT01 crystalline powder and 2wt.% Bi_2O_3 powder at a speed of 500 rpm for 5 h using a planetary ball mill with Teflon jar, zirconia balls, and 96% ethanol. The mixed powder was dried in an oven at 70°C for 3 h. The dried MZT01-2 powder was compacted using hydraulic-hand press and two cylindrical-die presses each with different diameters, namely 5 mm and 10 mm to produce pellets. The external pressure imposed on the 5-mm diameter pellets was at 2.5 MPa, while that of 10-mm diameter was at 20 MPa, each was held for 10 seconds to allow the air between the powders to escape. All pellets were sintered at 1000, 1100, and 1200°C for 4 h to obtain ceramics. The 10-mm diameter ceramics was aimed to perform the structure, microstructure, and bulk density characterization. While the 5-mm diameter ceramics, as required in Fig. 1, was to examine the resonance frequency of the ceramic when it was acting as a DRO material.

2. Data Collection and Processing

The structure data were obtained from XRD patterns measured using Bragg-Brentano Philips X'Pert Diffractometer with Cu-K_α radiation within 15-65° of diffraction angle and data steps of 0.02 °/minute. The XRD data were analyzed qualitatively and quantitatively. The qualitative analysis was carried out based on the *Search-and-match* method using *Match!* Software and powder diffraction file (PDF) database integrated with the software to identify crystalline phases formed in the ceramics. The quantitative analysis was performed using the Rietveld method and *Rietica* software to calculate the composition (quantitative data) of the identified crystalline phases.

Bulk density (ρ) data of the ceramics was measured based on the Archimedes method using Equation (2) and Mettler Toledo Balance type ME 403 E equipped with Density kit ME-DNY-43.[20]

$$\rho = \frac{m_d}{m_w - m_A}\rho_a \qquad (2)$$

where m_d is the dry mass of the ceramic, m_w is the wet mass of ceramic, m_A is Archimedes

mass of the ceramic, ρ_a is the density of aquades liquid used as the medium. The calculation in Eq. (2) was carried out by *Hyperterminal* software that was integrated with the measurement device.

Microstructure data comprising of surface morphology and grain and pore sizes were recorded from field emission scanning electron microscope using an FEI model Inspect F50 FESEM operating at 20 kV with the magnification of 5000x. The average diameter size of grains and pores on the microstructure images were measured using *ImageJ* software using in the following steps. First, select the scale to be used, in this case, the size of the bar scale on the FESEM image, i.e. 20 μm. Second, selecting the "Straight" button to measure the diameter of a particular grain or pore by drawing a straight line from several (i.e. eight) different positions. The measured diameter will be displayed automatically on the "Measurement" menu. Third, the average length of the straight lines measured from the 8 different positions can be obtained by averaging the data obtained. Figure 12a demonstrated the intended diameter measurement of grain from one position. The resonance frequency data of the ceramics when each ceramic was mounted as a resonator material in a DRO circuit was measured using a spectrum analyzer (Keysight MXA Signal Analyser N9020A) operating in $TE_{01\delta}$ mode within 3-12 GHz frequency range, 9-12 Volt, and 100-200 mA. All data in this study was plotted using *Origin* software.

Results And Discussion

1. Ceramic Structure

Figure 2 shows XRD patterns of the three MZT01-2 ceramics, each sintered at 1000, 1100, and 1200°C for 4 h.

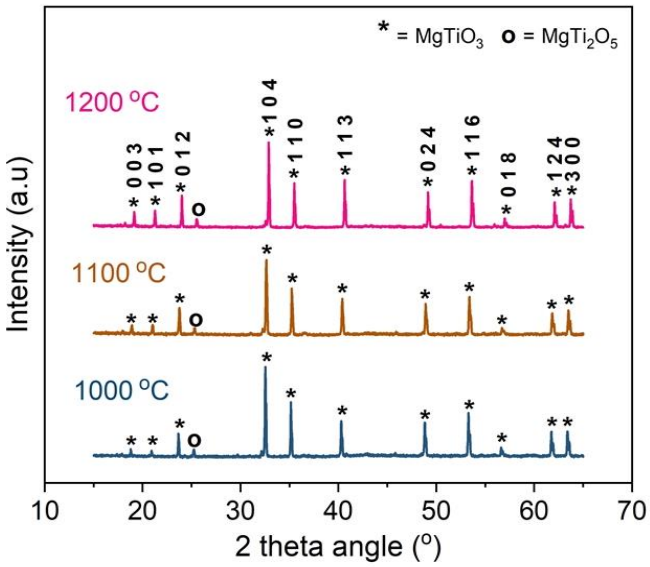

Figure 2. XRD patterns of MZT01-2 ceramics sintered at 1000, 1100, and 1200°C for 4 h.

In Figure 2, based on the phase identification results using *Match!* Software, it was obtained that there are two different phases resided in the samples, namely $MgTiO_3$ (PDF No. 06-0494), i.e. the peaks with (*) symbol on it and $MgTi_2O_5$ (PDF No. 35-0792), i.e. the minor peaks with (o) symbol on top.

Figure 3 shows the quantitative analysis (Rietveld refinement) result on the XRD pattern in Fig. 2, especially on the ceramic pattern sintered at 1000 °C to represent the same refinement result for the other two patterns. The refinement output data, i.e. molar % of the identified phases, parameters lattice, and unit cell volume of $MgTiO_3$ phase are given in Fig. 4-6.

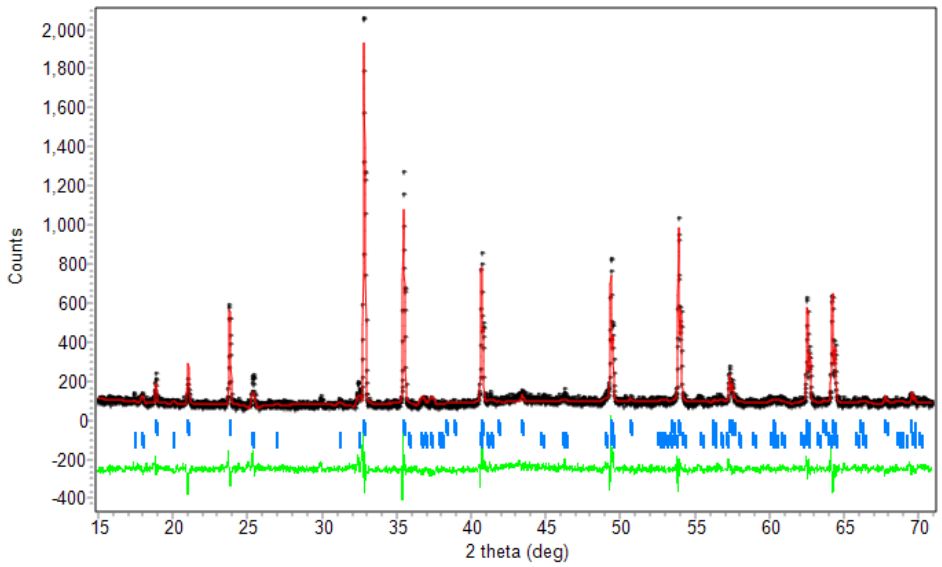

Figure 3. The Rietveld refinement on the XRD pattern of MZT01-2 ceramic sintered at 1000°C for 4 h in Fig. 2. (FoM: GoF = 2.30, R_p = 10.95, R_{wp} = 14.05, R_{exp} = 9.28)

In Fig. 3, the "+" symbol represents the experimental (measured) pattern, the red line is the model (calculated) pattern, the small blue upright lines are the position of the Bragg peaks belong to the two identified phases in Fig. 2. The green line represents the difference in the height of the diffraction peak intensity between the measured peak and the calculated peak. Figures of merit (FoM) represents the conformity values of the refinement results, consisting of the goodness of fit (GoF), the profile factor (R_p), the weighted profile factor (R_{wp}), and the experimental factor (R_{exp}).[21]

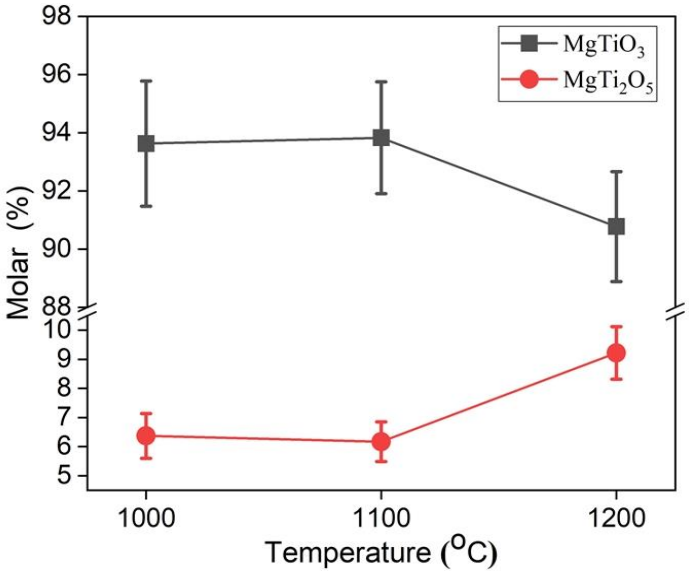

Figure 4. Molar % of $MgTiO_3$ and $MgTi_2O_5$ phases identified in the three ceramics in Fig. 2. The molar % data was the output of the Rietveld refinement in Fig. 3.

Based on Fig. 4, the three MZT01-2 ceramics contain the expected $MgTiO_3$ phase, i.e. (93.63±2.15), (93.83±1.92), and (90.78±1.89) % molar and the rest belongs to the $MgTi_2O_5$ phase. The increase of sintering temperature from 1000 to 1200°C tends to decrease the molar % content of the $MgTiO_3$ phase and, at the same time, increased the

$MgTi_2O_5$ content. According to Angela and Pratapa[22] the $MgTiO_3$ phase was formed via the reactions of $MgO+TiO_2 \rightarrow MgTiO_3$. According to Saukani et al, 2013 (23) in the fabrication of $(Mg_{0.8}Zn_{0.2})TiO_3$ ceramics, the $MgTi_2O_5$ phase that was identified to accompany the presence of the main phase of $MgTiO_3$ was very difficult to remove by heating so that when the sintering temperature was increased, the fraction of $MgTi_2O_5$ phase becomes even greater. This analysis was proven in this study.

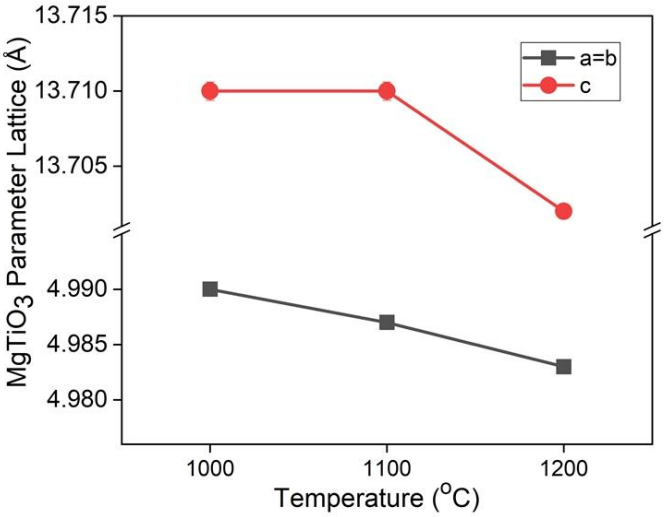

Figure 5. Parameters lattice of $MgTiO_3$ phase in the three MZT01-2 ceramics in Fig. 2. The data was the Rietveld refinement output in Fig. 3.

Based on Fig. 5, the c lattice parameters belong to the $MgTiO_3$ phase are relatively constant when the ceramics were sintered at 1000 and 1100°C, but the value significantly reduced at the temperature of 1200°C. While the a=b lattice parameter decreased constantly and in line with the sintering temperature from 1000 to 1200°C. The decrease in the lattice parameter value is similar to that in the unit cell volume in Fig. 6 considering that the size of $MgTiO_3$ unit cell volume was built from the size of the a and c lattice parameters in Fig. 5.

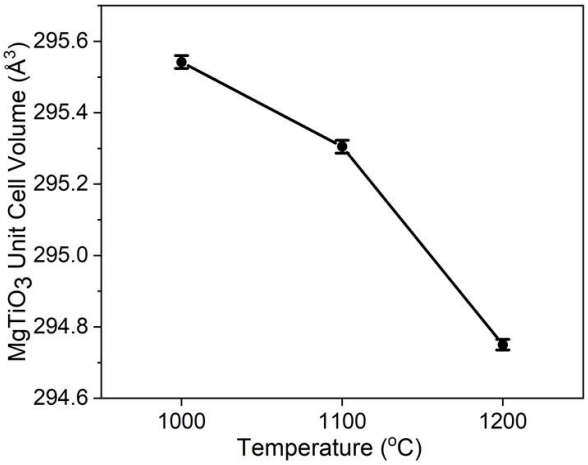

Figure 6. Unit cell volume of $MgTiO_3$ phase in the three ceramics in Fig. 2. The data was also the Rietveld refinement output in Fig. 3

Rahaman[24] explained that the process of sintering powder into ceramics generally occurs due to the diffusion of atoms in the microstructure. This diffusion of atoms occurs due to a difference in chemical potential, in this case, the atoms move from a spot with a higher chemical potential to another spot with lower chemical potential. The various paths

taken by atoms to move from one spot to another due to the chemical potential difference are referred to as the sintering mechanism, namely: surface diffusion, lattice diffusion from the surface, vapor transport, grain boundary diffusion, lattice diffusion from the grain boundary and plastic deformation. Among the six sinter mechanisms, not all of them cause the compaction process. The first three mechanisms are known as non-densifying mechanisms because these three mechanisms function to move the atoms from one surface of the particle and reposition them on another surface. In this case, the three mechanisms are only for repositioning the material in the pore and not causing the pore to shrink. While the remaining three mechanisms are called densifying mechanisms because they function to move the atoms from the bulk to the surface of the pores so that the pores disappear and the sample density increases.

Whereas in this study the MZT01-2 ceramic fabrication was carried out by adding a liquid additive agent (Bi_2O_3 powder) to the MZT01-2 powder. According to German[25] the sintering mechanism with the addition of a liquid additive agent consists of three stages, namely rearrangement, solution-precipitation, and final densification. The first stage occurs when the liquid phase melts, where the capillary force will pull the liquid into the pores. This force also causes the particles to reposition themselves more stable. The second stage occurs in areas that have high capillary pressure, i.e. places where particles are close to each other, the atoms prefer to enter the solution and then settle in areas that have lower chemical potential. This process compacts the system like the grain boundary diffusion mentioned above. The last stage, which is the compaction stage will occur in all parts of the system. German proposed that the shrinkage and densification which occurs due to diffused-controlled solution-precipitation is given in Equation 3.

$$\left(\frac{\Delta L}{L_o}\right)^3 = \frac{g\,\delta_L\,\Omega\,\gamma_{LV}\,D_s\,t\,C}{R\,T\,G^4} \qquad (3)$$

Where g is a geometric constant, δ_L is the thickness of the liquid layer between the particles, Ω is solid atomic volume, γ_{LV} is the surface energy between the solid-vapor, D_s is the degree of diffusion of the solid in the liquid, t is time, C is the solid concentration in the liquid, R is a gas constant, T is an absolute temperature and G is grain size which changes with sintering time.

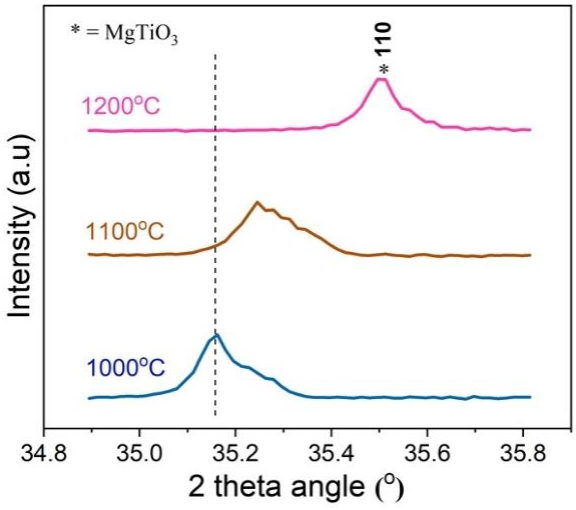

Figure 7. Zoom-in of the (110) diffraction peak at 2θ = 34.8 - 35.8° belonging to $MgTiO_3$ phase sintered at 1000, 1100, and 1200°C in Fig. 2.

As seen in Equation (3), there are so many factors affecting the shrinkage and densification of ceramics with a liquid additive agent. In this work, to collect

information on the effect of sinter temperature on the lattice parameter data in Fig. 5, an analysis involving the shift on the position of a diffraction peak (i.e. the position of the diffraction angle 2θ) belonging to the $MgTiO_3$ phase in Fig. 2 is required. In this case, the selected peak is the (110) peak located at 2θ = 34.8 - 35.8° (see Fig. 7).

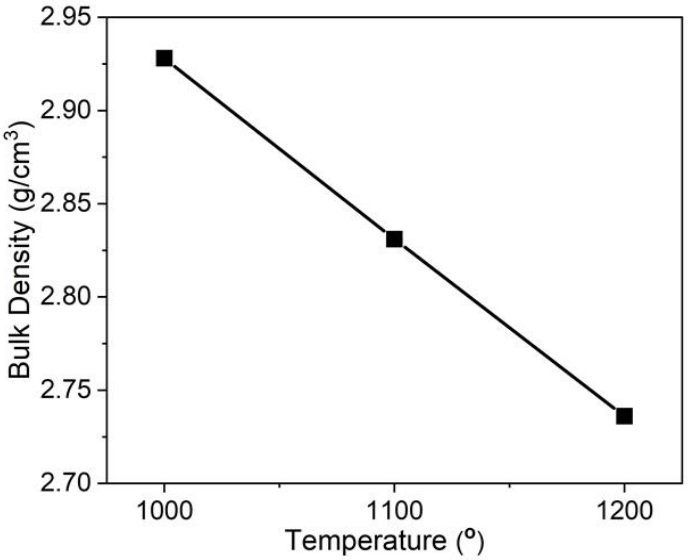

Figure 8. Bulk density of the three MZT01-2 ceramics

According to Fig. 7, the (110) peaks shifts to the right side, that is, towards a larger 2θ value due to the increase in sintering temperature from 1000 to 1200°C, i.e. from 35.1° at 1000°C, 35.3° at 1100°C and 35.5° at 1200°C. This fact can be deduced by involving Equations (4) and (5). Equation (4) shows the relationship between a = b and c lattice parameters and the distance between the two nearest crystal planes (d_{hkl}) in the $MgTiO_3$ phase, while Equation (5) is the Bragg's Law equation.[21]

$$\frac{1}{(d_{hkl})^2} = \frac{h^2+k^2}{a^2} + \frac{l^2}{c^2} \quad (4)$$

$$2\, d_{hkl} \sin\theta = n\lambda \quad (5)$$

where d_{hkl} is the distance between two nearest crystal planes at hkl orientation, a and c are lattice parameters, θ is Bragg angle, 2θ is diffraction angle, n is diffraction order, λ is the x-ray wavelength used. Based on Equation (4), when the parameters of lattice a=b and c are reduced (as sintering temperature increases) as in the case of this work, this gives rise to a decrease in d_{hkl} value. In Equation (5), the d_{hkl} value is inversely proportional to sinθ (which means that this value is also inversely proportional to sin2θ) so that when d_{hkl} is reduced, sin2θ becomes larger. This analysis is evident in Fig. 7, i.e. the 2θ position of (110) peak shifted towards a larger 2θ value as the sintering temperature increased from 1000 to 1200°C.

A decrease in ceramic density due to sintering was also reported by Akmal and Ramlan[26] on Na-β"-Al_2O_3 ceramic. It was explained that when the sintering holding time was increased, the pore sizes become larger since the gases needed to strengthen the bonds between atoms were burn or evaporated causing the density of the ceramic to decrease.

2. Bulk Density

Figure 8 presents the bulk density of the MZT01-2 ceramics that decreased from 2.928; 2.832 and 2.736 g/cm^3 as the sintering temperature increased.

This phenomenon could also be the case of bulk density decrease in Fig. 8, but it was not yet been confirmed in this work, especially when the phenomenon is confronted with Equation (3). The decrease in density in Fig. 8 may also relate to the decrease in unit cell volume in Fig. 6.

Bulk density of MZT01+2wt.% Bi_2O_3 ceramics reported by Zendya and Ermawati[18] increased along with the increase of compaction pressure from 10, 15, and 20 MPa, i.e. 2.8; 3.6; and 3.8 m/g^3. Based on Zendya and Ermawati[18] the bulk density of the ceramic due to variations in compaction pressure was much better than the density obtained in this work.

3. Microstructure

Figures 9-11 present microstructure data recorded from the fractured surface of the MZT01-02 ceramics sintered at 1000, 1100, and 1200°C for 4 h. As seen, the ceramic surface is very dense consisting of grain (inside red circle) of varying morphology and sizes, ranging from 1.9 to 2.3 μm, accompanied by some pores (inside blue squares). Fig. 12a demonstrates how to measure a diameter of grain using the *ImageJ* software, while Fig. 12b shows the average diameter of grains and pores measured from Fig. 9-11.

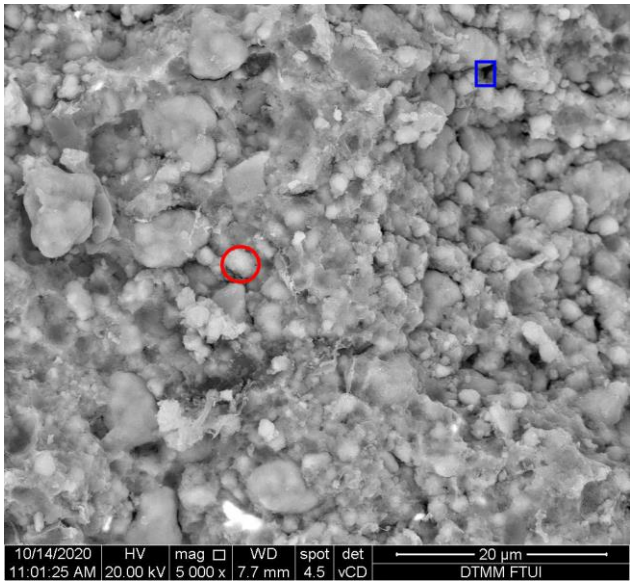

Figure 9. Microstructure of MZT01-2 ceramic sintered at 1000°C for 4 h with the magnification of 5000x

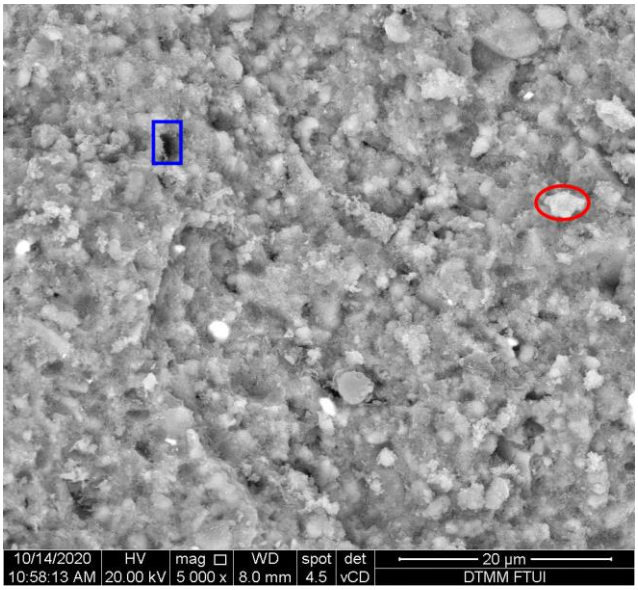

Figure 10. Microstructure of the ceramic sintered at 1100°C for 4 h with the magnification of 5000x

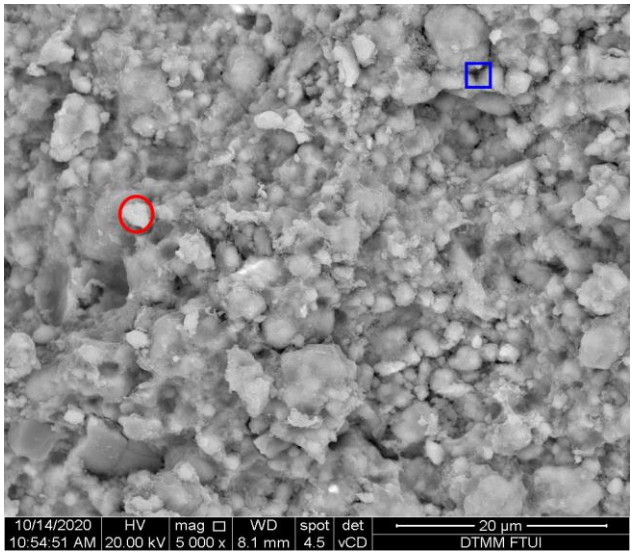

Figure 11. Microstructure of the ceramic sintered at 1200°C for 4 h with the magnification of 5000x

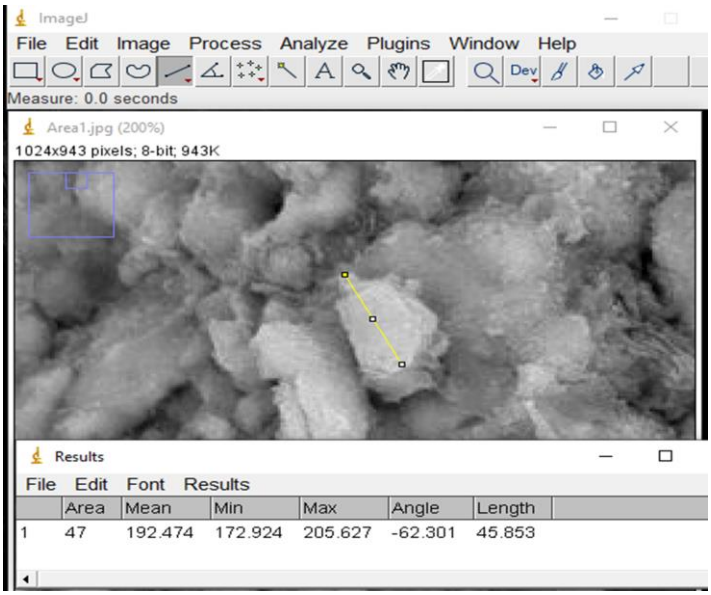

Figure 12a. zoom in a grain diameter measurement using the *ImageJ* software

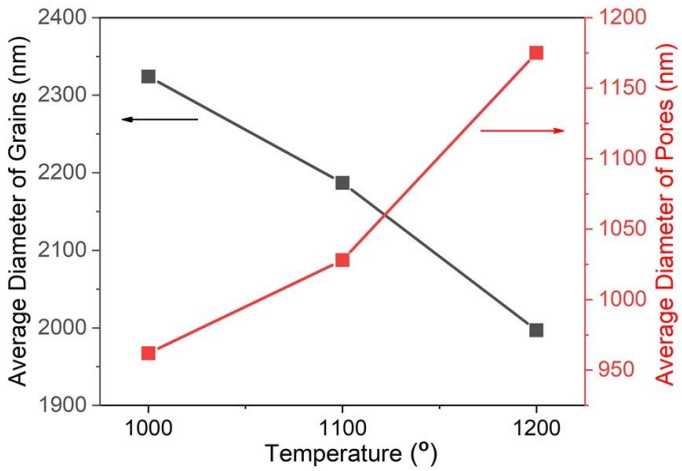

Figure 12b. The average diameter of grains and pores in MZT01-2 ceramics. The data was measured from Figs. 9-11.

Based on Fig. 12b, the average diameter of grains decreases as the sintering temperature increases, meanwhile the average pore sizes increase. The increase in the pore size is in line with the decrease in bulk density in Fig. 8.

4. MZT01-2 Ceramic Application as Resonator on DRO Circuit

Figure 13 shows the set-up of resonant frequency measurement for the MZT01-2 ceramic when the ceramic acts as a DRO material in the DRO circuit. The set-up consists of four main components, namely A, B, C, and D, where A = MZT01-2 ceramic as a DRO material, B = DRO circuit consisting of four parts as described in the Introduction section, C = a connector that connects B to the spectrum analyzer and D = two-pieces (red and black) connectors that connect B to the power supply, as also described in the Introduction section. Figure 14 depicts the results of the DRO resonance frequency measurement carried out in Fig. 13.

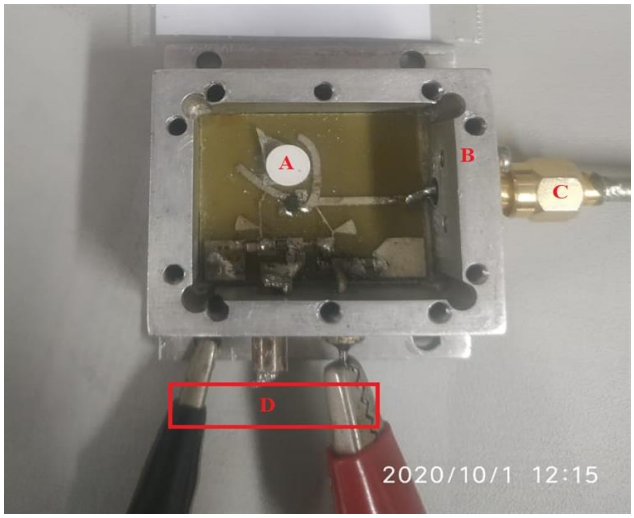

Figure 13. Set-up of resonance frequency measurement for MZT01-2 ceramics in the DRO circuit

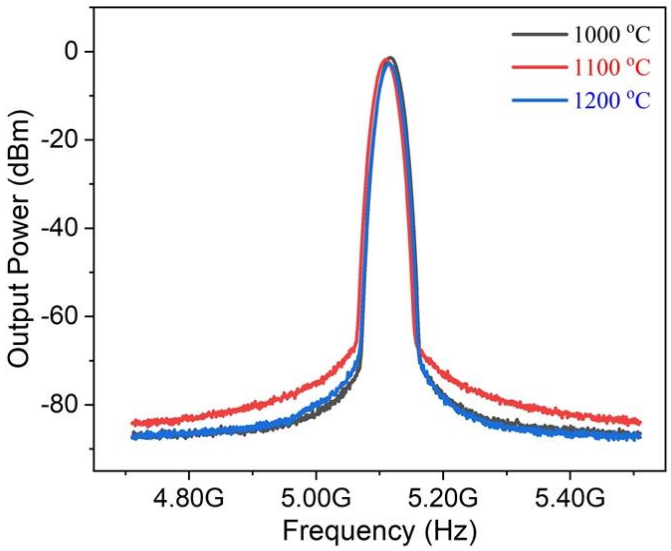

Figure 14. Resonance signal frequency of MZT01-2 ceramic as DRO material in DRO circuit.

In Fig. 14, the resonant frequency signals of the three ceramics are located in almost the same position as each other, i.e. at 5.11 GHz with the output power of -1.39 dBm (sintered at 1000°C), at 5.08 GHz with the output power of -1.83 dBm (at 1100°C) and 5.12 GHz with

the output power of -2.77 dBm (at 1200°C). The slight increase in the width of the tail of the resonance spectrum that appears on 1100°C ceramic has no physical meaning because the performance of a ceramic as a resonating material in the DRO circuit is more determined by where the resonant frequency is located and how much output power is generated. An ideal DRO resonator material is characterized by a sharp resonance spectrum with a very narrow width and near-zero output power. However, the ideal resonance spectrum is almost impossible to obtain considering that the ideal ceramic fabrication, i.e. perfect ceramics, without any defects at all is also difficult to do. The intended defects could be the co-presence of phases other than the expected phase, the presence of pores, low density, and so on. As seen in Fig. 14, the resonant frequency positions of the three spectra are similar (even overlapped) with each other. The output powers of the three resonance spectra are also equally close to zero, although the tail of 1100°C spectrum is slightly wider when compared to the tails of the other two spectra. Based on these facts, it can be concluded that the performance of the three ceramics as DRO resonator materials is as good as each other. These results confirm that the three ceramics fabricated in this work can be used as resonator materials (i.e. producing standing waves) in the DRO circuit operating in the microwave region. Figure 14 also confirms that the variation of sintering temperature does not affect the performance of the ceramic as a DRO material. Recently, Ermawati, 2021 (27) reported the performance of $(Mg_{0.6}Zn_{0.4})TiO_3$ ceramic as a DRO material at a slightly lower frequency of 4.7 GHz.

Conclusion

The work to fabricate MZT01-2 ceramics by varying sintering temperatures of 1000, 1100, and 1200°C, structural, microstructure, and bulk density characterization as well as to examine the use of the ceramics as DRO materials operating in microwave frequency has been completed. It was obtained that the three ceramics contain the main and desired phase, i.e. $MgTiO_3$. The ceramics have demonstrated their ability as a DRO resonator material in the microwave frequency region, particularly at ~5.1 GHz regardless of the sintering temperature.

References

1. Ermawati FU. Grain Size Analysis on Pure and Zn-doped Ilmenite Magnesium Titanane Powders. Omega J Fis dan Pendidik Fis. 2017;3(1):15–22.
2. Wu HT, Jiang YS, Cui YJ, Zhang XH, Jia X, Yue YL. Improvements in the sintering behavior and microwave dielectric properties of geikielite-type $MgTiO_3$ ceramics. J Electron Mater. 2013;42(3):445–51.
3. Wang H, Yang Q, Li D, Huang L, Zhao S, Xu S. Sintering Behavior and Microwave Dielectric Properties of $MgTiO_3$ Ceramics Doped with B_2O_3 by Sol-Gel Method. J Mater Sci Technol. 2012;28(8):751–5.
4. Zhang J, Yue Z, Luo Y, Li L. $MgTiO_3/TiO_2/MgTiO_3$: An ultrahigh-Q and temperature-stable microwave dielectric ceramic through cofired trilayer architecture. Ceram Int [Internet]. 2018;44(17):21000–3. Available from: https://doi.org/10.1016/j.ceramint.2018.08.135
5. Sheen J. A dielectric resonator method of measuring dielectric properties of low loss materials in the microwave region. Meas Sci Technol. 2008;19(5).
6. Jacob M V., Hartnett JG, Mazierska J, Krupka J, Tobar ME. Dielectric characterisation of Barium Fluoride at cryogenic temperatures using TE_{011} and quasi TE_{0mn} mode dielectric resonators. Cryogenics (Guildf). 2006;46(10):730–5.
7. Exxelia Temex. Exxelia - E7000 (Materials & Tuning Components > Dielectric Resonators). Dielectr Reson Datasheet [Internet]. 2015;129–41. Available from: https://exxelia.com/en/product/detail/636/e7000
8. Fusco VF, Dearn A. Dielectric Resonator Oscillators. Encycl RF Microw Eng. 2005;
9. Seçkin Uğurlu Ş. Dielectric resonator

oscillator design and realization at 4.25 GHz. ELECO 2011 - 7th Int Conf Electr Electron Eng. 2011;1–4.
10. Taryana Y, Sulaeman Y, Praludi T, Wahyu Y, Santiko AB. Design of 9.4 GHz Dielectric Resonator Oscillator with an Additional Single Stage Amplifier. Proceeding - 2018 Int Semin Intell Technol Its Appl ISITIA 2018. 2018;34:9–13.
11. Gonzales G. Foundation of Oscillator Circuit Design. bostonarctech house, inc. 2007;
12. Chiu T. Dielectric constant measurement technique for a dielectric strip using a rectangular waveguide. IEEE Trans Instrum Meas. 2003;52(5):1501–8.
13. Skyworks. Properties, Test Methods, and Mounting of Dielectric Resonators. 2017;2. Available from: https://cm-sitecore.skyworksinc.com//media/SkyWorks/Documents/Products/25012600/Properties_and_Mounting_of_Dielectric_Resonators_202803B.pdf. Retrieved February 11, 2020.
14. Ermawati et al. Blok diagram sirkuit DRO dan blok diagram pengukuran respon frekuensi dan daya luaran DRO pada C-band untuk keramik dielektrik ($Mg_{1-x}Zn_x$)TiO_3. Sertifikat Hak Cipta Republik Indonesia. No. Pencatatan 000203671, 2020.
15. Ermawati et al. Metode Fabrikasi Keramik Dielektrik ($Mg_{1-x}Zn_x$)TiO_3 sebagai Dielektrik Resonator Osilator yang bekerja pada Pita C. Paten Indonesia. No. Permohonan P00202006498, 04 Sept. 2020.
16. Rostianbudi, FY. dan Ermawati, FU. Fabrikasi dan karakterisasi struktur dan densitas keramik ($Mg_{0,5}Zn_{0,5}$)TiO_3+x wt.% Bi_2O_3 sebagai kandidat naterial dielektrik. J Inov Fis Indones. 2020;09(02):72–7.
17. Rettiningtyas, N dan Ermawati, FU. Sintesis dan Fabrikasi Keramik ($Mg_{0,8}Zn_{0,2}$)TiO_3+2 wt.% Bi_2O_3 sebagai bahan Dielektrik serta Karakterisasi Struktur dan Densitasnya akibat Variasi waktu tahan Sinter. J Inov Fis Indones. 2020;09(02):25–33.
18. Zendya, L and Ermawati, FU. Pengaruh variasi tekanan kompaksi terhadap mikrostruktur dan densitas keramik ($Mg_{0,9}Zn_{0,1}$)TiO_3+2 wt.% Bi_2O_3 hasil sintesis menggunakan metode pencampuran larutan. *J. Inov. Fis. Indones.* 2020;09; 145–51.
19. Nisa, D and Ermawati, FU. Fabrikasi keramik ($Mg_{0,6}Zn_{0,4}$)TiO_3+xwt.% Bi_2O_3 hasil sintesis dengan metode pencampuran larutan dan pengaruh variasi x wt.% Bi_2O_3 terhadap struktur dan densitas keramik. J Inov Fis Indones. 2020;09(02):15–20.
20. Rani SA dan Suasmoro. ($Mg_{0,8}Zn_{0,2}$)TiO_3 Ceramics synthesize as dielectric material by attritor mill mixing methods'. Thesis. FMIPA, Physics, Institut Teknologi Sepuluh November, Surabaya, 2016
21. Ermawati FU. Difraksi Sinar X: Teori dan Analisis Data Eksperimen. Surabaya: UNESA University Press. Sertifikat Hak Cipta Republik Indonesia. No. Pencatatan 000139628, 2018.
22. Angela R. dan Pratapa S. Sintesis $MgTiO_3$ dengan Variasi Temperatur Kalsinasi Menggunakan Metode Pencampuran Larutan. J Sains Dan Seni Its. 2012;1(1):73–5.
23. Saukani, M, Ermawati, FU. dan Pratapa S. Mekanisme perlambatan penyusutan dalam kajian sintering ($Mg_{0,8}Zn_{0,2}$)TiO_3. 2013;(October):10–1.
24. Rahaman MN. Ceramic processing and sintering, second edition. Ceram Process Sintering, Second Ed. 2017;1–875.
25. German RM, Suri P, Park SJ. Review: Liquid phase sintering. J Mater Sci. 2009;44(1):1–39.
26. Akmal J, Ramlan. karakterisasi konduktivitas, porositas dan densitas bahan keramik Na-β"-Al_2O_3 dari komposisi Na_2O 13% dan Al_2O_3 87% dengan variasi waktu penahanan. J Penelit Sains. 2008;11(3):544–511.
27. Ermawati FU. The Response of ($Mg_{0.6}Zn_{0.4}$)TiO_3 Ceramic System as A Dielectric Resonator Oscillator at C-Band. J Phys Conf Ser. 2021;1805(1):0–6.